



Contents lists available at [SciVerse ScienceDirect](http://www.sciencedirect.com)

Journal of Industrial and Engineering Chemistry

journal homepage: www.elsevier.com/locate/jiec



Removal of malachite green from aqueous solution by zinc oxide nanoparticle loaded on activated carbon: Kinetics and isotherm study

M. Ghaedi ^{a,*}, A. Ansari ^b, M.H. Habibi ^c, A.R. Asghari ^d

^a Chemistry Department, Yasouj University, Yasouj 75914-35, Iran

^b Department of Chemistry, Science and Research Branch, Islamic Azad University, Fars, Iran

^c Chemistry Department, University of Isfahan, Isfahan 81746-73441, Iran

^d Chemistry Department, Semnan University, Semnan, Iran

ARTICLE INFO

Article history:

Received 17 February 2013

Accepted 22 April 2013

Available online xxx

Keywords:

Malachite green

Zinc oxide nanoparticle loaded on activated carbon

Kinetics and isotherm study

ABSTRACT

In this research, a novel adsorbent, zinc oxide nanoparticle loaded on activated carbon (ZnO-NP-AC) was synthesized by a simple, low cost and efficient procedure. Subsequently, this novel material was characterized and identified by different techniques such as Brunauer, Emmett and Teller (BET), scanning electron microscopy (SEM), X-ray diffraction (XRD) and Fourier transform infrared spectroscopy (FT-IR) analysis. Unique properties such as high surface area ($>603 \text{ m}^2/\text{g}$) and low pore size ($<61 \text{ \AA}$) and average particle size lower than 100 \AA in addition to high reactive atom and presence of various functional groups make it possible for efficient removal of malachite green (MG). In batch experimental set-up, optimum conditions for quantitative removal of MG by ZnO-NP-AC was attained following searching effect of variables such as adsorbent dosage, initial dye concentration and pH. Optimum values were set as pH of 7.0, 0.015 g of ZnO-NP-AC at removal time of 15 min. Kinetic studies at various adsorbent dosage and initial MG concentration show that maximum MG removal was achieved within 15 min of the start of every experiment at most conditions. The adsorption of MG follows the pseudo-second-order rate equation in addition to interparticle diffusion model (with removal more than 95%) at all conditions. Equilibrium data fitted well with the Langmuir model at all amount of adsorbent, while maximum adsorption capacity was 322.58 mg g^{-1} for 0.005 g of ZnO-NP-AC.

© 2013 The Korean Society of Industrial and Engineering Chemistry. Published by Elsevier B.V. All rights reserved.

1. Introduction

Industrial effluents (main environmental pollution source) contain highly color dyes with large amount of organic solids [1]. The entrance of such pollutants to different water body cause generation of hazards to aquatic life by their ability to enhance mutagenic and carcinogenic effect. The dye containing waste water was produced by textile, paper and printing activities. Among various types of dyes (charge and structure) [2,3], the toxicity associated with very light intensity and molar absorptive compounds [4] and such effluents discharge has problems in both toxicological and environmental view [5]. Generally, presence of aromatics ring, metal ions and halides, especially chlorides in dyes structure increase their toxicity, carcinogenicity, genotoxicity, mutagenic and teratogenic property to living beings [6]. Aqueous media contaminated with heavy metal ions and dyes cause serious harm to aquatic life concern to their toxicity, chemical oxygen

demand and restriction of photosynthetic phenomena through reduction of light penetration [7,8]. Malachite green (MG) has numerous industrial applications (dyeing of silk, leather, plastics, paper and others) and their appearance lead to harmful for humans and animals following inhalation and/or ingestion [9] and produce toxicity to respiratory system and reduced fertility in humans [10]. The triphenylmethane dyes biodegradation due to presence of nitrogen in their back bone (generate carcinogenic, genotoxic, mutagenic and teratogenic problems) is a difficult task [11]. MG check complicated chemical structure (Fig. 1) has high resistance to light and oxidizing agents, while its removal based on biological treatment and chemical precipitation has low efficiency [12]. Conventional wastewater treatment protocol based on physico-chemical, chemical and biological process divided into different branches including coagulation and flocculation [13], adsorption [14], Biosorption [15], electrochemical techniques [16] and fungal decolonization [17]. Among these procedures, adsorption is applicable for large-scale biochemical and purification applications [18]. This technique benefit from unique properties such as simple design, using non toxic and low cost adsorbents and high efficiency. Characteristics and appropriate selection of adsorbent

* Corresponding author. Tel.: +98 741 2223048; fax: +98 741 2223048.

E-mail addresses: m_ghaedi@mail.yu.ac.ir, ghaedims@yahoo.com (M. Ghaedi).

Nomenclature

C_t	dye concentration (mg/L) at time (t)
Q_e	equilibrium adsorption capacity (mg g ⁻¹)
C_e	dye concentration (mg/L) at equilibrium
V	volume of solution (L)
W	weight of adsorbent (g)
k_1	rate constant of pseudo-first-order adsorption (min ⁻¹)
k_2	second-order rate constant of adsorption (mg g ⁻¹ min ⁻¹)
H	second-order rate constants (mg g ⁻¹ min ⁻¹)
α	initial adsorption rate (mg g ⁻¹ min ⁻¹)
β	desorption constant (mg g ⁻¹)
C	intercept of intraparticle diffusion (related to the thickness of the boundary layer)
K_{dif}	rate constant of intraparticle diffusion (mg g ⁻¹ min ^{-1/2})
F	fraction of solute adsorbed at any time t (mg g ⁻¹)
D_i	effective diffusion coefficient of adsorbate in adsorbent phase
r^2	radius of adsorbent particles (m)
Q_m	maximum adsorption capacity reflected a complete monolayer (mg g ⁻¹) in Langmuir isotherm model
K_a	Langmuir constant or adsorption equilibrium constant (L mg ⁻¹) that is related to the apparent energy of sorption
RL	dimensionless equilibrium parameter (separation factor)
K_F	isotherm constant indicate the capacity parameter (mg g ⁻¹) related to the intensity of the adsorption
N	isotherm constant indicate the empirical parameter (g L ⁻¹) related to the intensity of the adsorption
T	absolute temperature in Kelvin
R	universal gas constant (8.314 J K ⁻¹ mol ⁻¹)
B_1	related to the heat of adsorption ($B_1 = RT/b$)
b_T	constant related to the heat of adsorption
K_T	equilibrium binding constant
K	constant related to the adsorption energy at the D–R isotherm (mol ² kJ ⁻²)
Q_m	theoretical saturation capacity at the D–R isotherm
ε	Polanyi potential at the D–R isotherm
E	mean free energy of adsorption
A	isotherm constants in the Harkins–Jura adsorption isotherm
χ^2	chi-squared test statistic
$q_{e,exp}$	experimental data of the equilibrium capacity (mg g ⁻¹)
$q_{e,calc}$	equilibrium capacity obtained by calculating from the isotherm model (mg g ⁻¹)
R^2	correlation coefficient

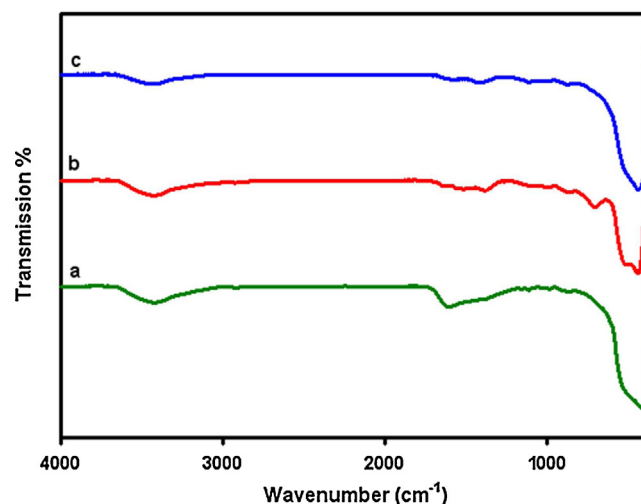


Fig. 1. FT-IR spectrum of ZnO nanoparticles annealed at (a) 350 °C, (b) 450 °C and (c) 550 °C.

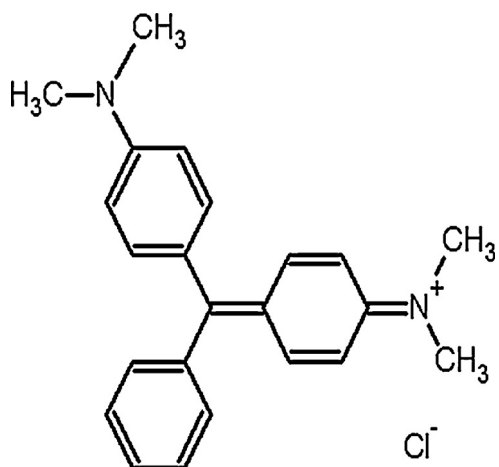
exchange capacity [20]. This study reports on the feasibility of applying ZnO-NP-AC as low-cost adsorbent for malachite green removal from aqueous solution. The effects of adsorbent dosage, initial MG concentration and pH on MG adsorption onto ZnO-NP-AC were studied. Adsorption kinetics and isotherms parameters were also evaluated and reported. The use of low-cost, non-toxic, high surface area as eco-friendly adsorbent has been investigated as an ideal alternative material for expensive and/or toxic adsorbent to removal malachite green (MG) from wastewater.

2. Experimental

2.1. Materials and instrumentation

The malachite green (Scheme 1), (C.I. Basic Green 4 C.I.) with classification Number of 42,000, chemical formula of C₂₅H₅₄N₄O₁₂ ($M_w = 927.00$) λ_{max} of 617 nm was supplied by Sigma–Aldrich (M) Sdn Bhd, Malaysia and used as received. The stock solution (100 mg/L) of MG was prepared by dissolving 50 mg of the MG in 500 ml distilled water. All working solutions with desired concentration prepared by diluting the stock solution with distilled water. Zinc acetate (ZA) dihydrate (99.9%), analytical reagent grade Isopropanol (IP) and monoethanolamine (MEA) (Sigma–Aldrich, Malaysia) was prepared by Sigma–Aldrich. The X-ray diffraction patterns (XRD) were recorded on a Bruker D8 advance X-ray diffractometer using the CuK α ($\lambda = 1.5406 \text{ \AA}$) radiation, with a scanning speed of 1° per min, 35 kV and 30 mA and 2θ scan over 2°–0°. The field emission scanning electron microscopy (FESEM) was performed on Hitachi, model S-4160, Japan. A BET surface analyzer (Quantachrome NOVA 2000, USA) was used to measure nitrogen adsorption–desorption isotherm at 77 K. Before each study, the samples were degassed via helium purging at 553 K for 3 h. The BET experiments give useful information on the adsorbent properties such as surface area, total pore volume and micropore area. The thermoanalytical measurements (TG-DTG) study for the thermal decomposition of precursors were carried out using a Mettler TA4000 system from 20 to 700 °C at a heating rate of 5 °C min⁻¹. UV-DRS spectra were recorded on a V-670, JASCO spectrophotometer, Tokyo, Japan. FT-IR absorption spectra of selected samples before and after heat treatment were obtained using KBr discs on a FT-IR 6300 in the region 4000–400 cm⁻¹ (Shimadzu FT-IR-8300 spectrophotometer, Shimadzu Co., Tokyo, Japan).

are based on remarks such as removal capacity, treatment cost and operating conditions [19]. Chemical treatment and biodegradation procedure are based on expensive and complex processes that generate toxic by-products. Using low cost, green and high adsorbent nanoparticles material are good approach that distinguish and distinct them in term of large surface area and high



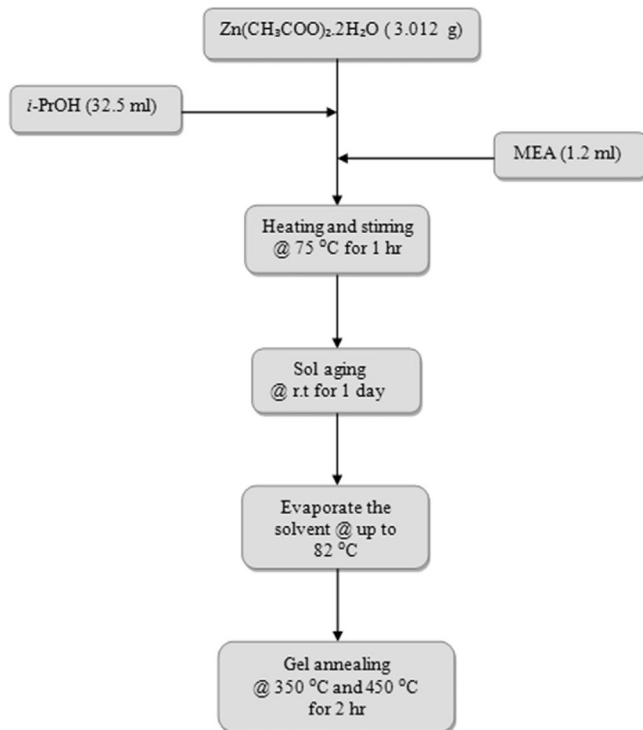
Scheme 1. Chemical structure of malachite green.

2.2. Sol–gel method for preparation of ZnO nanoparticles

Isopropanol solvent and monoethanolamine (MEA) was used to dissolve $(\text{CH}_3\text{COO})_2\text{Zn}\cdot 2\text{H}_2\text{O}$. The solution was heated under magnetic stirring at 75°C for 1 h to form a homogeneous sol solution. The obtained sol was stable for 1 day at room temperature. The respective stable sol was slowly heated under magnetic stirring up to 82°C until solvent evaporation to form a viscous homogeneous gel. After 1 day aging, the gel at room temperature was pyrolyzed and final gel was performed at temperature of 350 , 450 and 550°C for 2 h (Scheme 2). After the end of pyrolysis, the samples are sent for XRD, UV-DRS, FT-IR and FESEM examinations.

2.3. Adsorption studies

The batch sorption experiments were carried out in 100 mL Erlenmeyer flasks, where 0.005 – 0.02 g of the ZnO-NP-AC and



Scheme 2. Preparation of ZZN thin films coating on glass substrate (sol–gel method for preparation of pure ZnO).

50 ml of the MG solutions (5 – 30 mg/L) were added following pH adjustment. The Erlenmeyer flasks were subsequently capped and agitated for up to 35 min at 300 rpm in an isothermal shaker at room temperature to achieve equilibrium. The concentration of the MG in the solution after equilibrium adsorption was measured by a double beam UV-Vis spectrophotometer (Shimadzu, Model UV 1601, Japan) at 617 nm. The amount of adsorbed MG at equilibrium (q_e (mg g^{-1})) was calculated by:

$$q_e = \frac{(C_0 - C_e) V}{W} \quad (1)$$

where C_0 and C_e (mg/L) are the liquid-phase concentrations of dye at initial and equilibrium, respectively. V (L) is the volume of the solution and W (g) is the mass of dry adsorbent used.

To study the effect of solution pH, 0.015 g of ZnO-NP-AC was added to dye solution (50 ml, 15 mg/L) at room temperature in the pH range of 2 – 8 for isothermal shaking at 400 rpm for 35 min to achieve equilibration. The MG concentration in the solution after equilibrium was measured using calibration curve obtained at the same conditions. The pH was adjusted by addition of diluted 1.0 M NaOH and/or 0.1 N HCl before each experiment.

2.4. Adsorption kinetic studies

The effect of contact time in the 50 ml of MG solution with concentration in the range of 5 – 30 mg/L was examined by agitating solution via electromagnetic stirrer (Model 78-1) at room temperature at 300 rpm containing 0.005 – 0.02 g of ZnO-NP-AC homogeneously dispersed in solution. At predetermined time intervals (0 – 35 min) following centrifuge for 5 min a 4000 rpm the MG concentration was quantified and the actual amount of adsorbed MG at time t , q_t (mg g^{-1}), was calculated based on the following equation:

$$q_t = \frac{(C_0 - C_t) V}{W} \quad (2)$$

where C_0 and C_t (mg/L) are the concentrations of MG dye at initial and any time t , respectively. V (L) is the solution volume and W (g) represents the mass of adsorbent. The isotherm studies were performed by varying the initial MG concentrations at various adsorbent dosage and at all conditions, the amount of un-adsorbed MG was determined and actual equilibrium value of adsorbed MG was evaluated using Eq. (1).

3. Results and discussion

3.1. Characterization of ZnO-NP-AC

The characteristic functional groups of the adsorbent were investigated using FT-IR spectra as powerful identification tools. In Fig. 1 the broad absorption band observed at 3434 cm^{-1} corresponds to the O–H stretching vibrations of water present in ZnO and/or AC functional group. The FT-IR spectrum of present sorbent show high intensity of OH vibrations and lower contribution of CH_2 and CH_3 asymmetric and symmetric stretching vibrations. Two strong peaks observed in the range between 2963 and 2853 cm^{-1} are assigned to asymmetric and symmetric C–H bands of methyl and methylene groups. Stretching vibration band around 1700 cm^{-1} is assigned to carbonyl C=O group present in aldehyde, ester, ketone and acetyl derivatives. The strong band at 1600 cm^{-1} may be due to C=C band. Presence of such reactive atoms and metal center of zinc increase the number of vacant active sites for adsorptions [21]. The peaks appearing between 423 and 634 cm^{-1} are assigned to the metal–oxygen (M–O) stretching mode. In Fig. 1, the stretching mode of ZnO nanoparticles appears at 554 cm^{-1} . The room temperature DRS (UV–vis) absorption

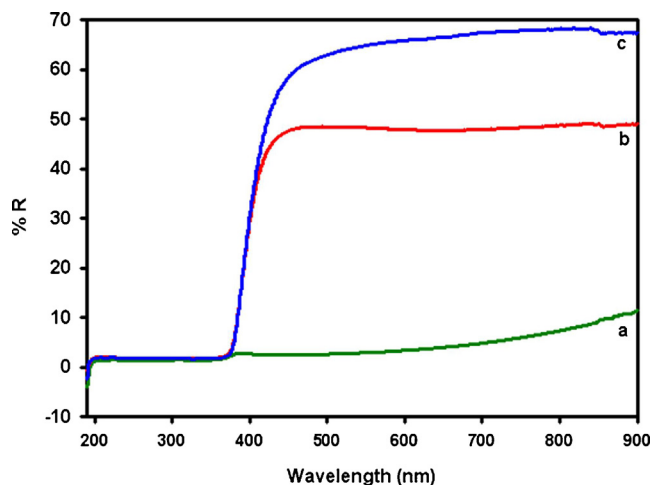


Fig. 2. UV-DRS reflectance spectra of ZnO nanoparticles annealed at (a) 350 °C, (b) 450 °C and (c) 550 °C.

spectrums for ZnO (Fig. 2) The Figure exhibits absorption edges in the range of 330–350 nm that its energy band gap was obtained using the following equation:

$$(\alpha h\nu)^2 = A(Eg - h) \quad (3)$$

where Eg represents the nanoparticles band gap and A is a characteristic constant. The band gap of this material generally evaluated according to intercept of line obtained by plotting $(\alpha h\nu)^2$ versus $h\nu$ t $(\alpha h\nu)^2 = 0$. The direct obtained band gap of ZnO was in the range of 3.53–3.44 eV that has difference with respective value of bulk ZnO (32 eV). Comparison of XRD pattern of powdered ZnO NRs with standard XRD pattern (Fig. 3) shows the appearance of peaks around 31.75°, 34.45°, 36.32°, 47.52°, 56.60°, 62.85°, 66.45°, 67.95° and 69.15° hexagonal structure of ZnO assigned to the planes (1 0 0), (0 0 2), (1 0 1), (1 0 2), (1 1 0), (1 0 3), (2 0 0), (1 1 2) and (2 0 1), respectively. Any diffracted peaks due to Zn(OH)₂ was not observed in the XRD pattern. The hexagonal structure lattice parameter was obtained from the d-interplanar spacing of different peaks by the equation:

$$1/d_{hkl}^2 = \frac{4}{3 \cdot (h^2 + hk + k^2)/a^2} + \frac{l^2}{C^2} \quad (4)$$

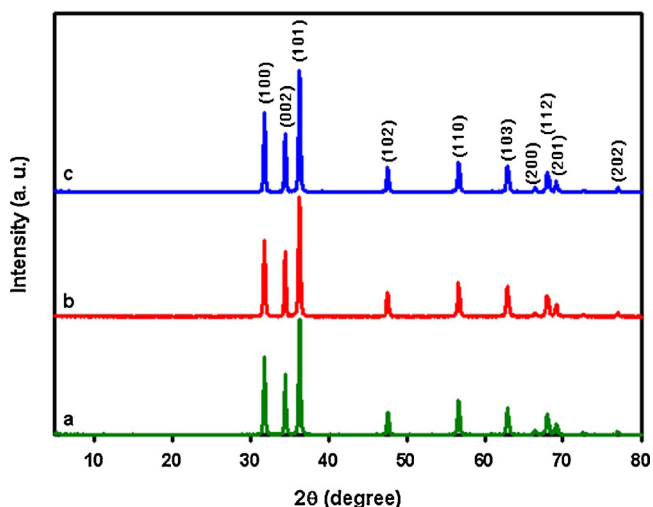


Fig. 3. XRD pattern of ZnO nanoparticles annealed at (a) 350 °C, (b) 450 °C and (c) 550 °C.

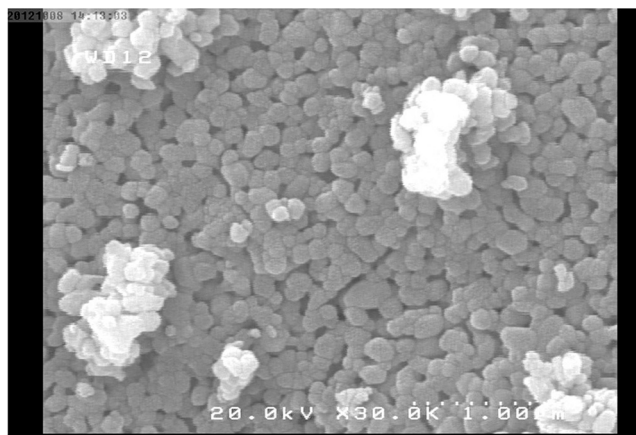


Fig. 4. FE-SEM image of ZnO nanoparticles annealed at 550 °C.

The mean values of $a=3.253$ and $c=5.208$ Å are in good agreement with the respective hexagonal values. The field emission scanning electron microscopy (FE-SEM) images of ZnO (Fig. 4) indicates randomly distributed nanoparticles with an average diameter of 46 nm. From the SEM analysis, it was found that there were holes and cave type openings on the surface of the adsorbent that accessible more surface area available for adsorption [22]. The particle surface becomes much smoother than that of the original particle following dye adsorption. Determination of specific surface area by N₂/77 K adsorption isotherms assumed to measure the surface area in micropores within pore sizes of a material [23]. Specific surface area (SSA) is the accessible area of adsorbent surface per unit mass of material. The interference by the surrounding phase is especially problematic for the Bruner–Emmet–Teller (BET) N₂ adsorption/desorption isotherm method because the entire surface is modified by vacuum treatment before N₂ adsorption. Table 1 and Figs. 5–9, show that adsorbent possessed appreciable narrow micro-porosity. The surface area of ZnO-NP-AC was found to be 603 m²/g. Total pore volume is 0.041 cm³/g and average pore diameter is less than 10 nm. Total surface properties of adsorbent are presented in Table 1.

3.2. Effect of contact time and initial MG concentration

The contact time necessary to reach equilibrium depends to the initial dye concentration and amount of adsorbent [24]. The relation between MG removal and stirring time were studied at various initial MG concentration and amount of adsorbents. The typical results of MG removal percentage at pH 7.0 at different contact time at 0.005 and 0.01 g of ZnO-NP-AC is presented in Figs. 10 and 11. It was found that more than 50% of MG removal occurs in the first 2 min at all initial concentration at higher value of adsorbent (>0.015 g). Subsequently, the adsorption rate changes slightly due to decrease in diffusion rate and concentration gradient. Later slow rate of MG adsorption is probably due to the electrostatic repulsion between the positive charges adsorbed molecules and respective ones in the bulk in coincide to the slow pore diffusion of the solute ions into the bulk of the adsorbent. It can be seen that the final equilibrium time significantly depend to the initial dye concentration and amount of adsorbent. At each initial dye concentration, the increases in adsorbent mass enhance the MG diffusion and subsequently decrease the time for complete dye removal. The equilibrium removal time at 5 and 30 mg/L for adsorbent mass of 0.015 g is in the range of 14 and 26 min, respectively. On the other hand, at 20 mg/L of MG by changing adsorbent weight from 0.005 to 0.02 g, the removal percentage was in the range of 96.3–99%. Also, the effect of initial

Table 1
 Summary report of adsorbent properties.

Summary report		
<i>Surface area</i>		
BET surface area		603.0782 m ² /g
BJH adsorption cumulative surface area of pores between 17.000 and 3000.000 Å width		188.955 m ² /g
BJH desorption cumulative surface area of pores between 17.000 and 3000.000 Å width		226.9081 m ² /g
<i>Pore volume</i>		
BJH adsorption cumulative volume of pores between 17.000 and 3000.000 Å width		0.288403 cm ³ /g
BJH desorption cumulative volume of pores between 17.000 and 3000.000 Å width		0.301245 cm ³ /g
<i>Pore size</i>		
Adsorption average pore width (4V/A by BET)		31.4561 Å
BJH adsorption average pore width (4V/A)		61.052 Å
BJH desorption average pore width (4V/A)		53.104 Å
<i>Nanoparticle size</i>		
Average particle size		99.490 Å

concentration of MG in the solution on the capacity and equilibrium time of removal process shown in Figs. 10 and 11. The experiments were carried out at various amount of adsorbent in the range of (0.005, 0.01, 0.015, 0.02 g) at room temperature (27 ± 2 °C), pH 7 and different initial concentrations of MG (5–30 mg/L) over time in the range of 0.5–35 min. It was observed that the removal percentage in despite of actual amount of adsorbed MG decrease with increase in initial dye concentration. The adsorption capacity at 0.005 till 0.02 g of ZnO-NP-AC was decrease from 322.58 to 76.9 mg g⁻¹. In the proposed process, the MG dye molecules initially must encounter the boundary layer effect and subsequently diffuse into the porous structure of the adsorbent over longer contact time. The MG molecule can diffuse to most adsorbent porous that this phenomenon takes relatively long time. A view glance to respective results, show that at each initial concentration by increasing the

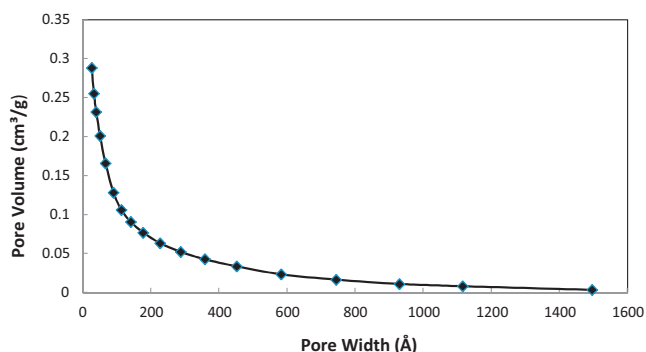


Fig. 5. BJH adsorption cumulative pore volume (larger) Halsey: Faas correction.

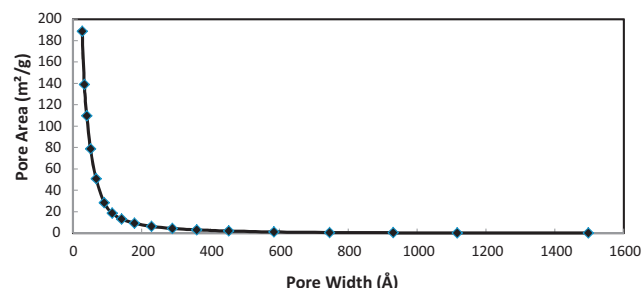


Fig. 6. BJH adsorption cumulative pore area (larger) Halsey: Faas correction.

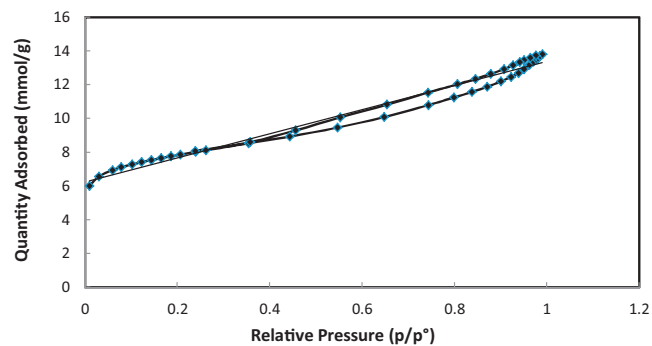


Fig. 7. Isotherm linear plot.

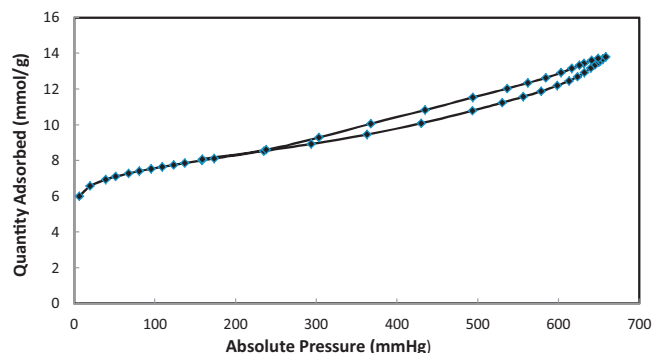


Fig. 8. Isotherm linear absolute plot.

amount of adsorbent, the removal time significantly reduced, while the adsorption capacity has opposite relation. At fixed adsorbent concentration, the increase in initial MG value lead to shortening equilibrium time and enhance in adsorption. As the initial MG concentration increases from 5 to 30 mg/L, its removal percentage decrease from 99.80 to 32.4% using 0.005 and 0.02 and most of the total MG amount removal occurs in the initial stirring time. In the first 10 min, the major portion of equilibrium adsorbed value is around 90–76 for initial MG concentrations of 5–30 mg/L using 0.005 g adsorbent, respectively, while at 0.02 g adsorbent the removal percentage was in the range of 96–99%. This observation is related to the high initial concentration gradient that represents high driving force for the MG transfer to the ZnO-NP-AC surface. It is also clear from typical curve (Fig. 13) that the required contact time for MG solutions with initial concentrations of 5–30 mg/L was less than 35 min at all conditions. Absolute amount of adsorbed MG has strong and positive correlation with initial MG concentration. It could be said that the higher the adsorbate concentration, the more diffusion would occur from the adsorbent surface into the microspore. So, the initial

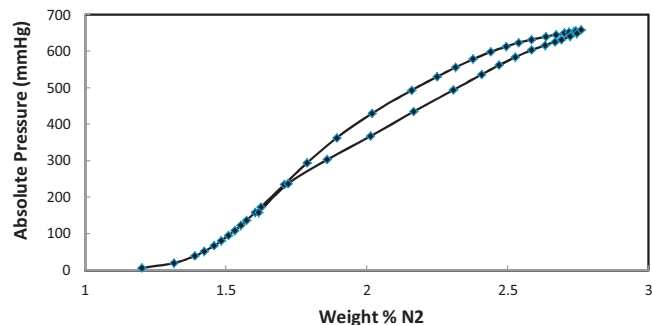


Fig. 9. Isotherm pressure composition.

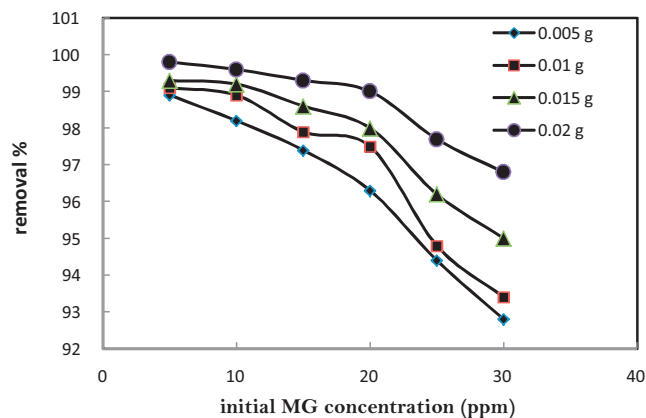


Fig. 10. Effect of initial dye concentration on the adsorption of MG.

rate of adsorption was greater for high initial MG concentrations and the resistance to the MG uptake diminished as the mass transfer driving force increased [25]. Increase in the adsorption with adsorbent dose can be attributed to increased adsorbent surface area and availability of more adsorption sites, while the unit adsorbed of MG decreased with increase in ZnO-NP-AC dose. This may be due to the decrease in total adsorption surface area available to MG resulting from overlapping or aggregation of adsorption sites [26].

3.3. Effect of system pH on MG uptake

The pH of the system exerts profound influence on the ability of adsorbent surface for interaction and dye molecule tendency for binding to solid surface. These phenomena presumably are due to its influence on the surface properties of the adsorbent and ionization/dissociation of the adsorbate molecule. Fig. 12 shows the variations in the MG removal from wastewater at different solution pH. It is evident, that the maximum removal of MG is observed at pH 7. The pH dependency of adsorption is attributed to the hydrophobic nature of the applied adsorbent which lead to absorption of hydrogen ions (H^+) onto the surface of the ZnO and/or AC when immersed in water and made it positive charge. At low pH (1.0–3.0), due to excess amount of H^+ ion concentration, the proposed adsorbent acquires positive charge. At higher pH value (above 7) the number of negatively charged sites enhance and a significantly strong electrostatic attraction appears between adsorbent and cationic MG molecule. The lowest adsorption occurred at pH 2.0 and the highest adsorption occurred at pH 7.0. The maximum q_e was observed at pH 7 and beyond it do not change significantly. No significant change in the adsorbed amount of dye was observed after pH 5 that suggest high dependency of

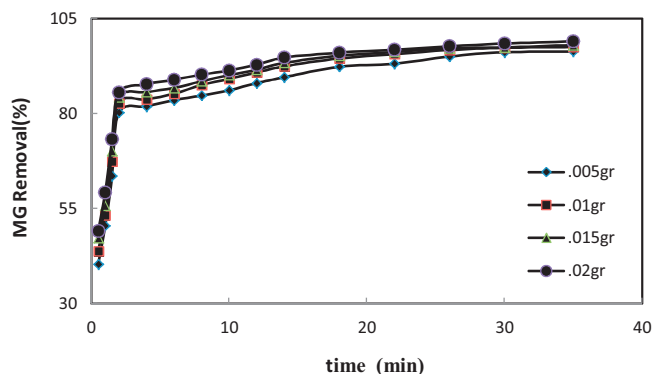


Fig. 11. Effect of contact time on the removal of different adsorbent of ZnO-NP-AC in concentration 20 mg/L of MG at pH 7.0.

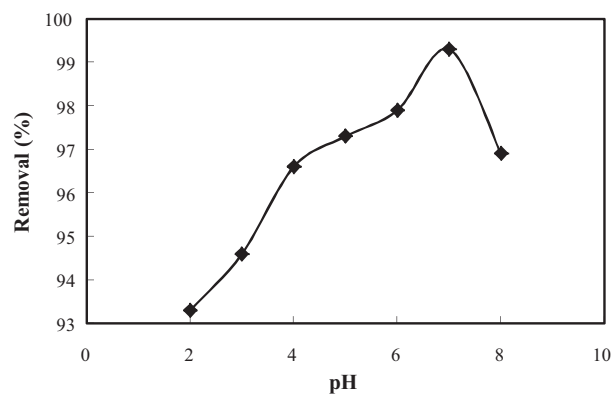


Fig. 12. Effect of system pH on adsorption of MG (15 mg/L) onto ZnO-NP-AC (0.015 g, 15 mg/L) at room temperature ($27 \pm 2^\circ C$), agitation speed 300 rpm for the maximum contact time required to reach the equilibrium (35 min).

removal to the adsorbent surface and the MG structure and charge. The behavior clearly indicates the probability of two pathways such as the dye protonation in acidic medium and its deprotonation with rise in pH. The first fact leads to formation of positive charge on adsorbent surface which inhibits from its tendency for interaction and adsorption of cationic dyes [27] (Fig. 10).

3.4. Equilibrium isotherms

Adsorption equilibrium isotherm represent mathematical relation of amount of adsorbed target per gram of adsorbent (q_e ($mg\ g^{-1}$)) to the equilibrium solution concentration (C_e (mg/L)) at fixed temperature. This investigation has great attention from both theoretical and practical point of view to obtain strong knowledge about surface properties of adsorbent and removal mechanism [28].

3.4.1. Langmuir isotherm

The theoretical Langmuir isotherm as one of most traditional model has maximum adsorption capacity corresponding to complete monolayer coverage on the adsorbent surface that calculated according to well know procedure [29]. A plot of C_e/q_e versus C_e at various amount of ZnO-NP-AC in the range of 0.005–0.02 g should indicate a straight line with slope of $1/Q_m$ and intercept equal to $1/k_a Q_m$. Depicting this line at various conditions (amount of ZnO-NP-AC) make possible to calculate the value of constant correspond to this model (Table 2). The high correlation coefficients and high maximum monolayer capacity ($322.6 - 76.9\ mg\ g^{-1}$ using 0.005–0.02 g adsorbent) show strong positive evidence on the fitness of equilibrium data of MG adsorption by Langmuir model (Table 2).

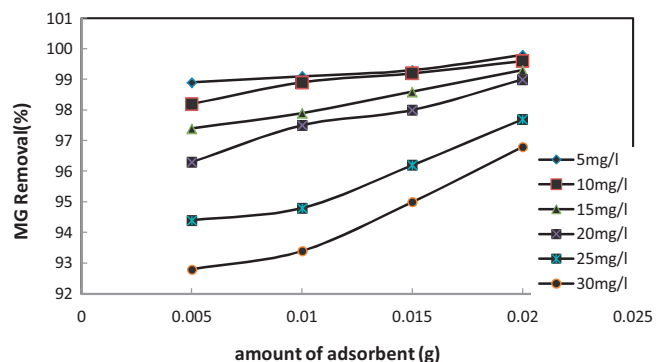


Fig. 13. Effect of adsorbent dosage on MG removals in the range of 0.005–0.02 g at (pH 7.0, agitation speed: 300 rpm, temperature: $27 \pm 2^\circ C$).

Table 2
Isotherm constants of MG adsorption onto ZnO-NP-AC.

Isotherm	Equation	Parameters	Adsorbent (g)			
			0.005	0.01	0.015	0.02
Langmuir	$C_e/q_e = 1/K_a Q_m + C_e/Q_m$	Q_m (mg g ⁻¹)	322.58	153.85	105.26	76.92
		K_a (L mg ⁻¹)	2.38	3.61	4.52	10.83
		RL	0.014–0.08	0.01–0.05	0.007–0.042	0.003–0.018
		χ^2	2.4503	0.967	0.356	0.1
		R^2	0.9897	0.9903	0.9918	0.9908
Freundlich	$\ln q_e = \ln K_F + (1/n)\ln C_e$	$1/n$	0.47	0.43	0.44	0.39
		K_F (L mg ⁻¹)	209.1	113.83	87.374	80.9
		χ^2	4.545	3.12	13.9	47.146
		R^2	0.9857	0.9604	0.9631	0.9707
Tempkin	$q_e = B_1 \ln K_T + B_1 \ln C_e$	B_1	62.47	29.68	20.2	13.44
		K_T (L mg ⁻¹)	32.01	47.72	62.33	186.24
		χ^2	11.7	6.25	12.85	35.088
		R^2	0.9828	0.9879	0.9928	0.9873
		E (kJ mol ⁻¹) = $1/(2K)^{1/2}$	4.08	4.08	5	7.07
Dubinin and Radushkevich	$\ln q_e = \ln Q_s - K\varepsilon^2$	Q_s (mg g ⁻¹)	232.04	122.4129	85.704	66.5398
		K	3.00E-08	3.00E-08	2.00E-08	1.00E-08
		χ^2	1062.125	1172.7	578.2	366.7
		R^2	0.9415	0.9697	0.9806	0.9815

3.4.2. The Freundlich isotherm

The Freundlich isotherm model [30] has constants such as K_F that show information about the bonding energy and know as the adsorption or distribution coefficient and represents the quantity of dye adsorbed onto adsorbent. $1/n$ show adsorption intensity of dye onto the adsorbent (surface heterogeneity). The value closer to zero by rising heterogeneous nature of surface ($1/n < 1$ indicates normal Langmuir isotherm while $1/n$ above 1 indicate bi-mechanism and cooperative adsorption). The applicability of the Freundlich adsorption isotherm was assessed by plotting $\log(q_e)$ versus $\log(C_e)$ and respective values for this model constants at various amount of adsorbent is shown in Table 2. The correlation coefficients (0.96–0.98) and higher error value of this model show that the Freundlich model has lower efficiency compare to the Langmuir model.

3.4.3. The Tempkin isotherm

Judgment for suitability of each model for the representation of methods applicability for explanation of experimental data is according to R^2 value and lower value concern to error analysis. Although, Langmuir and even Freundlich model have reasonable and acceptable R^2 value, but the applicability of other models such as Tempkin isotherm has commonly been applied in the following linear form [31,32]: The Tempkin isotherm Eq. (5) can be simplified to the following equation:

$$q_e = \beta \ln \alpha + \beta \ln C_e \quad (5)$$

where $\beta = (RT)/b$ is related to the heat of adsorption, T is the absolute temperature in Kelvin and R is the universal gas constant, 8.314 (J mol⁻¹ K⁻¹) [33,34]. The adsorption data were analyzed according to the linear form of the Tempkin isotherm Eq. (5). Examination of the data shows that the Tempkin isotherm is efficiently applicable for fitting the MG adsorption onto ZnO-NP-AC. The linear isotherm constants and coefficients of determination are presented in Table 2. The heat of MG adsorption onto ZnO-NP-AC was found to increase from 13.44 to 62.47 kJ mol⁻¹ with decrease in ZnO-NP-AC dose from 0.02 to 0.005 g. The correlation coefficients R^2 obtained from Tempkin model were comparable to that obtained for Langmuir and Freundlich equations, which explain the applicability of Tempkin model to the adsorption of MG onto ZnO-NP-AC. On the other hand according to χ^2 as a significant criterion most applicable model is Langmuir model.

3.4.4. The Dubinin–Radushkevich (D–R) isotherm

The D–R model was also applied to estimate the porosity, free energy and the characteristics of adsorbents [35,36]. The D–R isotherm dose not assumes a homogeneous surface or constant adsorption potential. The D–R model has commonly been applied in the following Eq. (6) and its linear form can be shown in Eq. (7):

$$q_e = Q_m \exp(-B\varepsilon^2) \quad (6)$$

$$\ln q_e = \ln Q_m - B\varepsilon^2 \quad (7)$$

where B is a constant related to the adsorption energy, Q_m the theoretical saturation capacity, ε the Polanyi potential, calculated from Eq. (8).

$$\varepsilon = RT \ln \left(1 + \frac{1}{C_e} \right) \quad (8)$$

The slope of the plot of $\ln q_e$ versus ε^2 gives B (mol²(kJ²)⁻¹) and the intercept yields the adsorption capacity, Q_m (mg g⁻¹). The mean free energy of adsorption (E), for transfer of one mole of target from infinity in solution to the surface of the solid was calculated from the B value using the following relation [37]:

$$E = \frac{1}{\sqrt{2B}} \quad (9)$$

The calculated value of D–R (Table 2) show that the model saturation adsorption capacity at optimum conditions using different amount of adsorbents was in the range of 232.04–66.5398, respectively, that has good agreement with respective Langmuir value. The values of E calculated using Eq. (9) is 4.08–7.07 kJ mol⁻¹ corresponding to physico-sorption process plays the significant role in the adsorption of MG onto ZnO-NP-AC. Another important criterion for evaluating applicability of each model was carried out using error analysis (χ^2). The non-linear chi-square test statistic (χ^2) [38], (the best-fit isotherm) is based on the following equation:

$$\chi^2 = \frac{\sum (q_{e,\text{exp}} - q_{e,\text{cal}})^2}{q_{e,\text{cal}}} \quad (10)$$

where $q_{e,\text{exp}}$ and $q_{e,\text{cal}}$ are experimental and calculated adsorption capacity value, respectively. The good agreement of

data acquired by each model need that, χ^2 value has smaller number and non-applicability of each model makes possible larger χ^2 value. The obtained non-linear value that higher r^2 value and smaller χ^2 value of Langmuir isotherm compared to the similar value of other applied models confirm its high efficiency to represent the experimental data at all conditions. The lower correlation coefficient (R^2) of Freundlich model in comparison to Langmuir model, suggest that the removal process better modeled by monolayer compare to multilayer adsorption. To confirm this result, the favorable or unfavorable MG adsorption onto Langmuir model was judged by calculation of the separation factor (RL) as follow [27].

$$RL = \frac{1}{(1 + K_a C_0)} \quad (11)$$

where K_a ($L\ mg^{-1}$) is the Langmuir constant and C_0 (mg/L) is the initial concentration. The adsorption process can be determined as favorable when the RL value lies between 0 and 1. It was found that for all adsorbent dosages and initial MG concentrations the RL value are lower than 1, suggest the favorable adsorption and good fitness of Langmuir model to explain experimental data. On the other hand increase in RL value with rising initial MG concentration and adsorbent dosage show high tendency of MG for adsorption onto ZnO-NP-AC.

3.5. Kinetic study

Every adsorption process may follow one or their combination from different patterns such as chemical reaction, diffusion control and mass transfer. Analysis of experimental date at various time make possible to calculate the kinetic parameters, (helpful for the prediction of adsorption rate) and take some information for designing and modeling the adsorption processes. The modeling of the kinetics of present removal studies was investigated by evaluation and analysis of the removal rate to various conventional models like the Lagergren pseudo-first-order model (Eq. (12)) [39], Ho's pseudo-second-order model (Eq. (13)) [40], and the Elovich model (Eq. (14)) [41].

$$q = q_e(1 - e^{-k_1 t}) \quad (12)$$

$$q = \frac{q_e^2 k_2 t}{(1 + q_e k_2 t)} \quad (13)$$

$$q = \frac{1}{\beta(\ln(1 + \alpha\beta t))} \quad (14)$$

where q_e is the amount of MG adsorbed at equilibrium ($mg\ g^{-1}$), q is the amount of MG adsorbed at time t ($mg\ g^{-1}$), k_1 is the rate constant of pseudo-first-order adsorption (min^{-1}), k_2 is the rate constant of pseudo-second-order adsorption ($g/mg\ min$), α is the initial adsorption rate ($mg\ g^{-1}\ min$) and β is the desorption constant (g/mg). The experimental kinetic results were modeled to above mentions situations and their estimated parameters values are shown in Tables 3–6. It despite of reasonable value of the R^2 correspond to pseudo-first-order model at 0.005 g adsorbent (R^2 : 0.8793–0.9349), but in comparison to experimental q_e values, the respective value of this model has great differences (73.3–57.84% deviation) and its value is higher at large MG concentrations. Good and reasonable fits of Lagergren's model at low MG concentration significantly deteriorates at higher concentrations. However, estimated q_e values of pseudo-second-order model accurately predict the adsorption kinetics over the entire working times. Therefore, this model has enough sufficiency for précis and acceptable accurate prediction of the kinetics of MG adsorption onto ZnO-NP-AC. The correlation coefficient (R^2) for the pseudo-second-order kinetic at different initial MG concentrations was above 0.992 and the calculated q_e values have good agreement to the experimental values (Tables 3–6). The equilibrium sorption capacity q_e in this study, increase from 50 to 277.78 $mg\ g^{-1}$ by raising the MG concentration from 5 to 30 mg/L at 0.005 g adsorbent. The Elovich model that has the poorest fitting at low concentrations and its efficiency for fitting and prediction of experimental data improves at higher MG concentrations [42]. The initial adsorption rates can be calculated from the pseudo-second-order model by the following equation:

$$h_{0,2} = k_2 q_e^2 \quad (15)$$

and the results are shown in Tables 3–6. The result notice that the initial adsorption rate increases with elevating the initial MG concentration and maximum value was obtained at maximum concentration. The initial increase in $h_{0,2}$ probably attributed to enhance in the mass transport driving force emerged from higher ratio of MG molecules to reactive vacant adsorbent sites. At higher concentrations due to apparent MG dimerization [43,44] and difficult diffusion of large dimmers in small adsorbent pores that cause to kinetic parameters worsened.

The slope and the intercepts of show the plots of $\log(q_e - q_t)$ versus t used for calculation of k_1 and q_e value and the numerical value of these parameters is shown in Tables 3–6. The difference between the $q_{e,calc}$ to the experimental data ($q_{e,exp}$) and low R^2 values (Tables 3–6) for the Lagergren model at different

Table 3
Kinetic parameters of MG adsorption onto ZnO-NP-AC conditions: 0.005 g adsorbent over 5–30 mg/L at optima conditions of other variables.

Parameter values: concentration dye (ppm)							
Models	Parameters	5	10	15	20	25	30
First order kinetic model: $\log(q_e - q_t) = \log(q_e) - (k_1/2.303)t$	k_1	0.09811	0.0889	0.0847	0.0735	0.0647	0.0534
	q_e (cal)	13.225	26.78	43.0427	65.1628	98.333	125.661
	R^2	0.9349	0.8976	0.8793	0.888	0.9145	0.8912
Second-order kinetic model: $t/q_t = 1/k_2 q_e^2 + (1/q_e)t$	$k_2 \times 10^2$	0.0282	0.0133	0.0082	0.0052	0.0031	0.0025
	q_e (cal)	50	100	149.254	196.078	243.902	277.78
	R^2	0.9996	0.9996	0.9997	0.9993	0.9984	0.9969
	H	70.4225	133.33	181.82	200	185.185	196.078
Intraparticle diffusion $q_t = K_{id} t^{1/2} + C$	K_{dif}	3.473	7.496	12.21	16.928	22.629	26.486
	C	32.421	61.891	87.596	109.29	121	137.35
	R^2	0.6871	0.6833	0.7051	0.7178	0.7941	0.7772
Elovich $q_t = 1/\beta \ln(\alpha\beta) + 1/\beta \ln(t)$	β	0.2008	0.0927	0.0572	0.0416	0.0319	0.0273
	R^2	0.8656	0.8673	0.886	0.8882	0.9329	0.9139
Experimental date	q_e (exp)	49.95	99.87	149.77	199.49	248.77	298.05

Table 4

Kinetic parameters of MG adsorption onto ZnO-NP-AC conditions: 0.01 g adsorbent over 5–30 mg/L at optima conditions of other variables.

Parameter values: concentration dye (ppm)							
Models	Parameters	5	10	15	20	25	30
First order kinetic model: $\log(q_e - q_t) = \log(q_e) - (k_1/2.303)t$	k_1	0.104	0.0993	0.0866	0.0845	0.0638	0.0587
	q_e (cal)	5.824	12.674	19.240	29.587	44.823	56.247
	R^2	0.9324	0.933	0.8807	0.8981	0.9143	0.8911
Second-order kinetic model: $t/q_t = 1/k_2q_e^2 + (1/q_e)t$	$k_2 \times 10^2$	0.0672	0.0296	0.0191	0.0119	0.0073	0.0058
	q_e (cal)	25.063	50.25	74.63	99.01	120.48	142.86
	R^2	0.9997	0.9997	0.9997	0.9996	0.9987	0.9987
	H	42.194	74.627	106.383	116.279	106.383	119.047
Intraparticle diffusion $q_t = K_{dif} t^{1/2} + C$	K_{dif}	1.6026	3.4339	5.5556	8.1416	10.305	12.903
	C	17.038	32.778	46.816	58.093	66.056	74.686
	R^2	0.6556	0.677	0.681	0.7065	0.7926	0.7782
Elovich $q_t = 1/\beta \ln(\alpha\beta) + 1/\beta \ln(t)$	β	0.430	0.2020	0.1247	0.086	0.0701	0.0556
	R^2	0.846	0.8621	0.8693	0.8838	0.9312	0.9263
Experimental date	$q_e(\text{exp})$	24.98	49.96	74.905	99.825	124.43	149.11

Table 5

Kinetic parameters of MG adsorption onto ZnO-NP-AC conditions: 0.015 g adsorbent over 5–30 mg/L at optima conditions of other variables.

Parameter values: concentration dye (ppm)							
Models	Parameters	5	10	15	20	25	30
First order kinetic model: $\log(q_e - q_t) = \log(q_e) - (k_1/2.303)t$	k_1	0.1073	0.1018	0.0905	0.0866	0.0652	0.0613
	q_e (cal)	3.434	7.464	11.463	18.252	26.38	35.075
	R^2	0.9278	0.9233	0.8894	0.8989	0.8882	0.8945
Second-order kinetic model: $t/q_t = 1/k_2q_e^2 + (1/q_e)t$	$k_2 \times 10^2$	0.1188	0.0529	0.033	0.01966	0.01314	0.0096
	q_e (cal)	16.722	33.445	50	66.225	80.645	96.154
	R^2	0.9999	0.9998	0.9998	0.9997	0.9989	0.9986
	H	33.22	59.172	82.645	86.21	85.47	88.496
Intraparticle diffusion $q_t = K_{dif} t^{1/2} + C$	K_{dif}	0.9922	2.1256	3.3914	5.0903	6.3418	8.0865
	C	11.808	22.818	33.019	40.664	47.719	53.345
	R^2	0.6247	0.6443	0.6508	0.6946	0.735	0.7632
Elovich $q_t = 1/\beta \ln(\alpha\beta) + 1/\beta \ln(t)$	β	0.6875	0.3225	0.2023	0.1370	0.112	0.0885
	R^2	0.8229	0.84	0.847	0.8748	0.8946	0.9128
Experimental date	$q_e(\text{exp})$	16.6567	33.3133	49.9567	66.5733	83.0567	99.55

concentrations show failness of this model to explain experimental data over all time and concentration.

The values of the rate constant were found to decrease from 2.82×10^{-2} to 2.5×10^{-3} g/mg min by raising the initial MG concentration from 5 to 30 mg/L at 0.005 g adsorbent. The conformity between experimental data and the model predicted

values was expressed by the correlation coefficients (R^2 values close or equal to 1) and between two first models another judgment is based on the agreement between experimental and theoretical experimental value. Comparison based on these two parameters show applicability of pseudo-second-order model for evaluating and fitting experimental data over entire adsorption

Table 6

Kinetic parameters of MG adsorption onto ZnO-NP-AC conditions: 0.02 g adsorbent over 5–30 mg/L at optima conditions of other variables.

Parameter values: concentration dye (ppm)							
Models	Parameters	5	10	15	20	25	30
First order kinetic model: $\text{Log}(q_e - q_t) = \log(q_e) - (k_1/2.303)t$	k_1	0.1227	0.1112	0.102	0.099	0.0755	0.0716
	q_e (cal)	2.485	5.05	8.004	13.143	16.368	22.84
	R^2	0.9379	0.927	0.9097	0.9263	0.8682	0.898
Second-order kinetic model: $t/q_t = 1/k_2q_e^2 + (1/q_e)t$	$k_2 \times 10^2$	0.1805	0.0834	0.0505	0.0285	0.0222	0.0153
	q_e (cal)	12.563	25.1256	37.594	50.25	61.728	73.529
	R^2	0.9999	0.9998	0.9999	0.9997	0.9996	0.9993
	H	28.49	52.632	71.43	71.94	84.746	82.645
Intraparticle diffusion $q_t = K_{dif} t^{1/2} + C$	K_{dif}	0.6757	1.4376	2.3727	3.6223	4.5399	5.7348
	C	9.2291	17.987	25.854	31.892	38.684	43.829
	R^2	0.5954	0.5979	0.6188	0.6799	0.673	0.7325
Elovich $q_t = 1/\beta \ln(\alpha\beta) + 1/\beta \ln(t)$	β	1.002	0.4706	0.2836	0.1914	0.1526	0.1233
	R^2	0.7973	0.8005	0.8219	0.8671	0.8598	0.8976
Experimental date	$q_e(\text{exp})$	12.4975	24.9925	37.485	49.965	62.3725	74.785

Table 7
Comparison of performance of proposed method with some previously reported MG adsorption systems.

Adsorbent	Adsorption capacity (mg g ⁻¹)	Contact time	Adsorbent dose	Source
Cyclodextrin-based material	91.9	120 min	0.15 g	[54]
Rice husk	76.92	60 min	0.6 g	[55]
Lignite activated carbon	149	60 min	–	[56]
Oil palm trunk fiber	149.35	120 min	–	[57]
Bentonite clay	7.72	10 min	0.05	[20]
Chitosan bead	93.55	300 min	–	[58]
Sawdust carbon	74.1	15–120 min	0.2–1.0 g	[59]
CAC Merck	222.22	30 min	0.01–0.1 g	[60]
Rubber wood sawdust	25.8–36.3	–	–	[47]
Hen feather	10.3–10.7	90 min	0.15 g	[48]
Commercial activated carbon	8.27	15 min	20 g	[49]
Laboratory grade activated carbon	42.18	15 min	4 g	[49]
Arundo donax root carbon	8.69	180 min	0.15–1.0 g	[50]
Lemon peel	3.2–51.7	24 h	0.05 g	[51]
Activated charcoal	0.179	30 min	0.01 g	[61]
Neem sawdust	4.354	14 min	2.517 g	[62]
AC from pine sawdust	370.37	3 h	0.1 g	[63]
Carbonaceous material	75.08	6–8 h	–	[64]
ZnO-NP-AC	322.58	0.5–30 min	0.005 g	This study

stage [45]. The values of initial sorption (h) proportional to initial rate of adsorption, increase from 70.4225 to 196.078 mg (g min)⁻¹ with the increase in initial MG concentrations from 5 to 30 mg/L for example at 0.005 g adsorbent (Tables 3–6).

3.5.1. The intraparticle diffusion model

The linear relation of initial dye concentration with removal rate failed when pore diffusion is the predominant stage and limits the adsorption process. The MG transfer from bulk to the solid phase through intraparticle diffusion/transport process known as rate-limiting step in especially in rapidly stirred batch process [46]. Therefore, the possibility and usability of this model for interpretation of experimental data was explored according to its well known equation and conditions:

$$q_t = K_{\text{dif}} t^{0.5} + C \quad (16)$$

where C (mg g⁻¹) is the intercept and K_{dif} is the intraparticle diffusion rate constant (in mg g⁻¹ min^{-1/2}). The values of q_t were found to be linearly correlated with values of $t^{1/2}$ and the rate constant K_{dif} directly evaluated from the slope of the regression line (Tables 3–6). The values of intercept C (Tables 3–6) provide information about the thickness of the boundary layer and, the external mass transfer resistance. The constant C was found to increase from 32.421 to 137.35 with increase in MG amount from 5 to 30 mg/L at 0.005–0.02 g of ZnO-NP-AC. This change in value is belong to increase in thickness of the boundary layer and decrease the chance of the external mass transfer and subsequently prominent increase in the amount of internal mass transfer. The high value of R^2 shows suitability of this model to explain the experimental data. This may confirm that the rate-limiting step is the intraparticle diffusion process. The intraparticle diffusion rate constant, (K_{dif}) value was in the range of 3.473–26.486 mg g⁻¹ min^{-1/2} at 0.005 g adsorbent and has good positive correlation with initial dye concentration. This linear relationship shows high contribution of intraparticle diffusion on the adsorption process. Generally, in kinetic studies passing the interparticle diffusion plot through origin show that this mechanism solely limits the adsorption rate [42]. This situation was not achieved in our study that shows the contribution of other pathway in addition to intraparticle diffusion model to follow the adsorption data.

3.6. Comparison with other adsorbents for MG

Many MG removal process using various biosorbent and adsorbents were reported in the literature [47–51] and their

performance for MG removal was compared in term of low-cost adsorbents amount of adsorbent and contact time. It can be seen that MG removal by ZnO-NP-AC (Table 7) is superior to previously reported literature in term of higher adsorption capacity (322.58 mg g⁻¹) shorter required time (15 min) and using small amount of adsorbent (0.015 g).

3.7. Mechanism of adsorption

Practical applications of adsorption depend to the dynamic behavior of the system. Where F is the fractional attainment of equilibrium at different times (t) and Bt is a function of F as follows:

$$F = \frac{q_t}{q_e} \quad (17)$$

where q_t and q_e are the dye uptake (mg g⁻¹) at time t and equilibrium, respectively. Performing the Fourier transformation and subsequent integration of Eq. (17) by Reichenberg [52] make possible to obtain the following approximations:

$$\text{for } F \text{ values} > 0.85, \quad Bt = -0.4977 - \ln(1 - F) \quad (18)$$

$$\text{and for } F \text{ values} < 0.85, \quad Bt = (\sqrt{\pi} - \sqrt{\pi} - \left(\frac{\pi^2 F}{3}\right)^2) \quad (19)$$

B can be used to calculate the effective diffusion coefficient, (D (cm²/s)) from the Eq. (18) as follows:

$$B = \frac{\pi^2 D_i}{r^2} \quad (20)$$

where r is the radius of the adsorbent particle assuming spherical shape. Eqs. (17)–(20) can be used to predict the rate limiting steps of adsorption process. The linear plot of B_t against time is linear and has zero intercept, when the pore diffusion controls the rate of mass transfer (Fig. 14) Nonlinear or linear relationship with intercept value different than the zero show that film-diffusion or chemical reaction controls the adsorption rate. On the other hand, Webber's pore-diffusion model is another single-resistance model that was derived from Fick's second law of diffusion based on well known assumptions such as external resistance, (i) to high initial; (ii) the radial and the concentration diffusion; (iii) and constant pore diffusivity and not-dependency to time. The pore diffusion parameter, k_i (mg g⁻¹ min^{0.5}) is defined by:

$$q_t = K_{\text{dif}} t^{0.5} + C \quad (21)$$

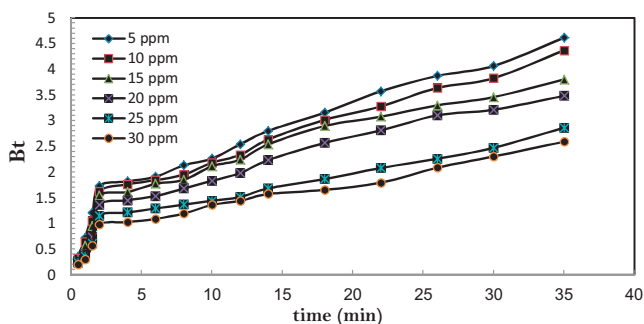


Fig. 14. Boyd plots for MG adsorption on ZnO-NP-AC at room temperature and different initial MG concentrations.

Table 8

Diffusion coefficients for adsorption of MG on ZnO-NP-AC at 25 °C and different initial concentrations.

C_0	K_{i1}	Intercept	K_{i2}
5	0.851	-0.0907	0.091
10	0.725	-0.0543	0.085
15	0.661	-0.0634	0.072
20	0.729	-0.2218	0.0698
25	0.1411	0.4257	0.0549
30	0.1063	0.4004	0.0493

where q is the amount of adsorbed MG (mg g^{-1}) at time t . It equation show that solely role of pore diffusion to limit mass transfer need that a plot of q against $t^{0.5}$ give straight line with a slope of k_i and the intercept value of C that represents the resistance to mass transfer in the external liquid film. It is clear that the plots are multi-linear. In multi-linear plots with non-zero intercept for the first lines show that pore diffusion is not the controlling stage of the overall rate of mass transfer, especially at first stages. Another competitive stage is film-diffusion that may taken place and ended in the initial stages of adsorption (from 0 to 5 min) or maybe it is still controlling the rate of mass transfer at time concern to first linear segment. The plots are linear in the initial period removal time and their slopes significantly differ from zero. These phenomena show that pore diffusion is not the sole rate limiting process. For adsorption time shorter than 5 min, film-diffusion or chemical reaction may be controlling the overall rate of adsorption. The presence of two pore diffusion periods suggest the existence of (k_{i1} and k_{i2}) represent the MG diffusion in to the pores have two distinct sizes (macropores and mesopores) [53]. Therefore, the decrease in value of k for macro -pore to mesopore diffusion is a direct consequence of the relative free path for diffusion available in each pore size (Table 8). Reduce in pore size lead to decrease in path available for diffusion consequently decreases in the rate of diffusion. At higher concentration of MG the pore diffusion rate parameters increases due to the increase in the bulk liquid dye concentration and improvement in its driving force.

4. Conclusion

This investigation show the efficiency of ZnO-NP-AC as a good, green and low-cost with high adsorption capacity adsorbent (322.58 mg g^{-1}) for the removal of MG from aqueous solutions in short time (<20 min). In this study, the effective pH was 7 and the optimum adsorbent dose was found to be 0.015 g . Langmuir isotherm gave a better fit to adsorption isotherms than Freundlich isotherm. The kinetic study of MG on ZNO-NP-AC was performed based on pseudo-first-order, pseudo-second-order, Elovich and

intraparticle diffusion equations. The results data indicate that the adsorpt follow the pseudo-second-order rate in addition to interparticle diffusion model. The present study concludes that the ZNO-NP-AC could be employed as low-cost adsorbents instead of commercial activated carbon for the removal of MG from water and wastewater. Further studies on quantitative characterization of this adsorbent and involved mechanisms, and feasibility of using this adsorbent for other dyes for possible industrial application are needed.

References

- [1] G. Crini, *Bioresource Technology* 97 (2006) 1061.
- [2] G. Mishra, M. Tripathy, *Colourage* 40 (1993) 35.
- [3] Y. Fu, T. Viraraghavan, *Bioresource Technology* 79 (2001) 251.
- [4] M. Ghaedi, S.H. Hajati, B. Barazesh, F. Karimi, G.H. Ghezalbash, *Journal of Industrial and Engineering Chemistry* 216 (2012) 119.
- [5] M. Ghaedi, Sh Heidarpour, S. Nasiri Kokhdan, R. Sahraie, A. Daneshfar, B. Brazesh, *Powder Technology* 228 (2012) 18.
- [6] T. Robinson, G. McMullan, R. Marchant, P. Nigam, *Bioresource Technology* 77 (2001) 247.
- [7] A. Sari, M. Tuzen, *Journal of Hazardous Materials* 160 (2008) 349.
- [8] O. Ozdemir, M. Turan, A.Z. Turan, A. Faki, A.B. Engin, *Journal of Hazardous Materials* 166 (2009) 647.
- [9] S.J. Culp, F.A. Beland, *Journal of the American Colloid Toxicology* 15 (1996) 219.
- [10] S. Srivastava, S. Rangana, D. Roy, *Aquatic Toxicology* 66 (2004) 319.
- [11] L. Papinutti, N. Mouso, F. Forchiassin, *Enzyme and Microbial Technology* 39 (2006) 848.
- [12] O. Dogan Uluozlu, A. Sari, M. Tuzen, M. Soylak, *Bioresource Technology* 99 (2008) 2972.
- [13] R.P. Han, J.H. Zhang, W.H. Zou, J. Shi, H.M. Liu, *Journal of Hazardous Materials* 125 (2005) 266.
- [14] V.K. Gupta, I. Ali, D. Suhas, Mohan, *Journal of Colloid Interface Science* 265 (2003) 257.
- [15] A. Sari, D. Mendil, M. Tuzen, M. Soylak, *Chemical Engineering Journal* 144 (2008) 1.
- [16] K.V. Kumar, *Journal of Hazardous Materials* 136 (2006) 197.
- [17] Y.S. Ho, *Water Research* 40 (2006) 119.
- [18] R. Dolphen, N. Sakkayanwong, P. Thiravetyan, W. Nakbanpote, *Journal of Hazardous Materials* 145 (2007) 250.
- [19] C. Kannan, T. Sundaram, T. Palvannan, *Journal of Hazardous Materials* 157 (2008) 137.
- [20] S.S. Tahir, N. Rauf, *Chemosphere* 63 (2006) 1842.
- [21] A.N.A.E.I. Hendawy, *Journal of Analytical and Applied Pyrolysis* 75 (2006) 159.
- [22] S.D. Khattri, M.K. Singh, *Indian Journal of Chemical Technology* 6 (1999) 112.
- [23] T.W. Ahmad, T.H. Usmani, M. Mumtaz, *Pakistan Journal of Science and Industrial Research* 24 (1991) 121.
- [24] M. Ghaedi, M. Nejadi Biyareh, S. Nasiri Kokhdan, S.H. Shamsaldini, R. Sahraei, A. Daneshfar, S. Shahriyar, *Materials Science Engineering: C* 32 (4) (2012) 725.
- [25] M. Ghaedi, A. Hekmati Jah, S. Khodadoust, R. Sahraei, A. Daneshfar, A. Miandoost, M.K. Purkait, *Spectrochimica Acta Part A: Molecular and Biomolecular Spectroscopy* 90 (2012) 22.
- [26] V.K. Garg, R. Kumar, R. Gupta, *Dyes Pigments* 62 (2004) 1.
- [27] M. Ghaedi, H. Hossainian, M. Montazerzohori, A. Shokrollahi, F. Shojai pour, M. Soylak, M. Purkait, *Desalination* 281 (2011) 226.
- [28] M. Ghaedi, *Spectrochimica Acta Part A: Molecular and Biomolecular Spectroscopy* 94 (2012) 346.
- [29] M. Dogan, M. Alkan, O. Demirbas, Y. Ozdemir, C. Ozmetin, *Chemical Engineering Journal* 124 (2006) 89.
- [30] Freundlich H.M.F., *Zeitschrift fur Physikalische Chemie (Leipzig)* 57A (1906) 385.
- [31] C. Aharoni, D.L. Sparks, *Soil Science Society America Journal* (1991) 1.
- [32] X.S. Wang, Y. Qin, *Process Biochemistry* 40 (2005) 677.
- [33] G. Akkaya, A. Ozer, *Process Biochemistry* 40 (11) (2005) 3559.
- [34] C.I. Pearce, J.R. Lloyd, J.T. Guthrie, *Dyes Pigments* 58 (2003) 179.
- [35] M.M. Dubinin, *Chemical Reviews* 60 (1960) 235.
- [36] M.M. Dubinin, *Zhurnal Fizicheshoi Khimii* 39 (1965) 1305.
- [37] L.V. Radushkevich, *Zhurnal Fizicheshoi Khimii* 23 (1949) 1410.
- [38] Y.S. Ho, A.E. Ofomaja, *Process Biochemistry* 40 (2005) 3455.
- [39] S. Kundu, A.K. Gupta, *Colloid Surfaces A: Physicochemical and Engineering Aspects* 273 (2006) 121.
- [40] S. Lagergren, *Handlingar* 24 (4) (1898) 1.
- [41] Y.S. Ho, G. McKay, *Water Research* 34 (2000) 735.
- [42] T. Santhi, S. Manonmani, T. Smitha, *Journal of Hazardous Materials* 179 (2010) 178.
- [43] C. Aharoni, D.L. Sparks, S. Levinson, I. Ravina, *Soil Science Society America Journal* 55 (1991) 1307.
- [44] N. Strataki, V. Bekiari, P. Lianos, *Journal of Hazardous Materials* 146 (2007) 514.
- [45] M. Ghaedi, B. Sadeghian, A. Amiri Pebdani, R. Sahraei, A. Daneshfar, C. Duran, *Chemical Engineering Journal* 187 (2012) 133.
- [46] G. McKay, *Chemical Engineering Journal* 27 (1983) 107.
- [47] K.V. Kumar, S. Sivanesan, *Dyes Pigments* 72 (1) (2007) 124.
- [48] A. Mittal, *Journal of Hazardous Materials* 133 (1–3) (2006) 196.

- [49] I.D. Mall, V.C. Srivastava, N.K. Agarwal, I.M. Mishra, *Colloids Surfaces A: Physico-chemical and Engineering Aspects* 264 (1–3) (2005) 17.
- [50] J. Zhang, L.I. Yan, Chenglu Zhang, Yuming Jing, *Journal of Hazardous Materials* 150 (3) (2008) 774.
- [51] K. Kumar, Vasanth, *Dyes Pigments* 74 (3) (2007) 595.
- [52] D. Reichenberg, *Journal of the American Chemical Society* 75 (1953) 589.
- [53] S.J. Allen, G. McKay, K.Y.H. Khader, *Environmental Pollution* 56 (1989) 39.
- [54] G. Crini, H.N. Peindy, F. Gimbert, C. Robert, *Separation and Purification Technology* 53 (2007) 97.
- [55] I.A. Rahman, B. Saad, S. Shaidan, E.S. Sya Rizal, *Bioresource Technology* 96 (2005) 1578.
- [56] Y. Önal, C. Akmil-Basar, C. Sarıcı-Özdemir, *Journal of Hazardous Materials* 146 (2007) 194.
- [57] B.H. Hameed, M.I. El-Khaiary, *Journal of Hazardous Materials* 154 (2008) 237.
- [58] Z. Bekci, C. Özveri, Y. Seki, K. Yurdakoc, *Journal of Hazardous Materials* 154 (2008) 254.
- [59] V.K. Garg, R. Gupta, A. Bala Yadav, R. Kumar, *Bioresource Technology* 89 (2003) 121.
- [60] R. Malik, D.S. Ramteke, S.R. Wate, *Waste Management* 27 (2007) 1129.
- [61] M.J. Iqbal, M.N. Ashiq, *Journal of Hazardous Materials* 139 (2007) 57.
- [62] S.D. Khattri, M.K. Singh, *Journal of Hazardous Materials* 167 (2009) 1089.
- [63] C. Akmil-Basar, Y. Onal, T. Kilicer, D. Eren, *Journal of Hazardous Materials* 127 (2005) 73.
- [64] V.K. Gupta, S.K. Srivastava, D. Mohan, *Industrial Engineering Chemistry Research* 36 (1997) 2207.